# Triple hourglass Weyl phonons

Guang Liu,[1] Zhongjia Chen,[1,2] Peng Wu,[1] and Hu Xu[1,3,*]

[1]*Department of Physics, Southern University of Science and Technology, Shenzhen 518055, People's Republic of China*

[2]*Songshan Lake Materials Laboratory, Dongguan, Guangdong 523808, People's Republic of China*

[3]*Quantum Science Center of Guangdong–Hong Kong–Macao Greater Bay Area (Guangdong), Shenzhen 518045, People's Republic of China*

(Received 7 September 2022; accepted 8 December 2022; published 19 December 2022)

Unconventional Weyl phonons with higher topological charges in crystalline solids have attracted increasing attention. By symmetry analysis and a low-energy $\mathbf{k}\cdot\mathbf{p}$ effective Hamiltonian, we propose the symmetry-enforced triple hourglass Weyl phonons (THWPs) with Chern number $\mathcal{C}=\pm3$ protected by $6_3$ screw rotation symmetry in chiral space groups 173 ($P6_3$) and 182 ($P6_322$). We take $LiIO_3$ with space group 173 as a candidate and confirm that it possesses THWP with linear and quadratic dispersions along the $k_z$ direction and in the $k_x$-$k_y$ plane, respectively. Due to the constraints of crystal symmetry and topological charge conservation, six equivalent single Weyl phonons (SWPs) emerge and lie in the $k_z=0$ plane. Therefore, the unique phonon surface arcs connect the projections of two THWPs and six SWPs, leading to nontrivial sextuple-helicoid surface arcs on the (001) surface Brillouin zone. Our work proposes a class of topological phonons and realizes it in realistic materials, providing a perfect platform for experimental observation of THWPs. We expect our work to provide a new idea for detection of unconventional quasiparticles.

DOI: 10.1103/PhysRevB.106.214308

In recent years, various topological quasiparticles in three-dimensional (3D) crystalline solids, such as Weyl points [1–3], triple points [4–6], Dirac points [7–11], nodal lines [12–15], and nodal surfaces [16–18], have attracted widespread attention because of their unique physical properties and potential applications. Among them, Weyl-type excitations are of particular importance, which are peculiar quasiparticle excitations featuring a nontrivial isolated point touching two band branches. Weyl fermions were first predicted theoretically in the magnetic pyrochlore iridates [19]. However, due to the limitation of magnetic domains of these magnetic materials, some typical physical properties of Weyl points are difficult to observe experimentally [20–22]. Fortunately, nonmagnetic materials with well-defined surface states and Fermi arcs were later proposed and observed experimentally [23–27].

Motivated by these works, more works on Weyl-type excitations have been reported. According to the band dispersion around crossing points which can lead to exotic topological properties, the Weyl-type points exhibit a variety of classification. For example, according to degree of the tilt of the local dispersion around the crossing, Weyl points are divided into type-I [3,19,23–28], type-II [29–34], and type-III Weyl points [35–37]. The latter two break the Lorentz symmetry, resulting in unique transport properties different from type-I Weyl points with normal pointlike Fermi surfaces [29–34]. In addition, the Weyl points, which act as a "source" or "sink" of Berry curvature [38], are topologically protected by the discrete translational symmetry of the lattice and no further symmetries are needed for their existence. Therefore, the topology of Weyl point can be defined by a quantized topological charge (i.e., the Chern number $\mathcal{C}=\pm1$), which is the flux of the Berry curvature passing through a closed surface in momentum space. However, considering an additional symmetry, there will exist some Weyl points with higher Chern number $\mathcal{C}$ [39–48]. For example, a fourfold or sixfold rotation symmetry can protect Weyl points with $\mathcal{C}=\pm2$ [5,39–42], a sixfold rotation symmetry can protect Weyl points with $\mathcal{C}=\pm3$ [2,43], and Weyl points with $\mathcal{C}=\pm4$ [45–48] can be realized when the cubic symmetry is included in the presence of threefold screw rotational symmetry. Under this convention, Weyl points are divided into single Weyl, quadratic Weyl, triple Weyl, and charge-four Weyl points with $\mathcal{C}=\pm1$, $\pm2$, $\pm3$, and $\pm4$, respectively.

Phonons can be a perfect platform for realization of these unconventional Weyl points due to their particular device applications and the unique advantages of whole frequency range observation. For example, quadratic Weyl phonons (QWPs) can exist with two equal single Weyl phonons (SWPs) in $\alpha$-$SiO_2$ [41]. Unlike paired SWPs with opposite chiral charges, the projection of the QWP connects two SWPs by two surface arcs. More importantly, such a combination does not violate the no-go theorem [49,50] and satisfies topological charge conservation. The charge-four Weyl (CFW) point was proposed only in the spinless system [45–47], and the quadruple-helicoid surface states are available. However, the studies focusing on topological nontrivial triple Weyl phonons (TWPs) are still in their infancy, and the TWPs with clearly visible surface states have so far not been realized in realistic materials. As shown in Fig. 1(a), we propose the existence of the TWP with exotic triple-helicoid surface states, which connect the projections of the TWP and three SWPs. Interestingly, sextuple-helicoid surface states in

*xuh@sustech.edu.cn

 

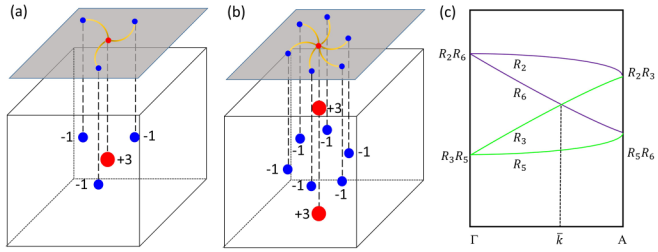


FIG. 1. (a) The schematics of a triple Weyl point with triple-helicoid surface arcs. (b) The schematic of a pair of triple Weyl points connected by time-reversal symmetry with sextuple-helicoid surface arcs. (c) The schematic of the hourglass band dispersion on a $6_3$-invariant screw axis.

Fig. 1(b) can be expected when two TWPs are connected by time-reversal symmetry $\mathcal{T}$. However, the TWPs originate from the accidental degeneracies on a $C_6$-invariant line, and therefore we cannot explicitly distinguish it from SWPs and QWPs on the same path. Then a questions arises: Is there some kind of constraint that guarantees the existence of TWPs on high-symmetry lines (HSLs)? The hourglass-shaped band structures, which may result in symmetry-enforced intersection, such as hourglass nodal points and nodal lines [51–55], would be a good choice to realize the TWPs. Therefore, a class of exotic topological phase, i.e., the triple hourglass Weyl phonons (THWPs), can be expected.

Through $\mathbf{k}\cdot\mathbf{p}$ effective model analysis, we identified all candidate space groups (SGs) capable of possessing TWPs, which are listed in Table S1 of the Supplemental Material (SM) [56]. On this basis, by analyzing the evolution of the irreducible representations (IRs) on $C_6$-invariant HSLs, we find that SGs 173 and 182 can host the THWPs with $\mathcal{C}=\pm3$ in our candidate SGs, which originate from the different screw rotation degrees of the $C_6$. Therefore, we divide the triple Weyl phonons into general TWPs and THWPs. Taking $LiIO_3$ as an example, we confirm the nontrivial topological properties of THWPs and find they possess unique sextuple-helicoid surface arcs on the (001) surface, which is consistent with our prediction. It should be stressed that the THWP is enforced to appear by symmetry, and its hourglass band characteristics makes it easier to be observed and detected.

To understand the properties of TWPs, the crossings of two phonon branches can be described by a two-band $\mathbf{k}\cdot\mathbf{p}$ effective Hamiltonian, namely,

$$\mathcal{H}(\mathbf{k}) = d(\mathbf{k})\sigma_+ + d^*(\mathbf{k})\sigma_- + f(\mathbf{k})\sigma_z, \tag{1}$$

where $\sigma_{x,y,z}$ are Pauli matrices, $\sigma_\pm=(\sigma_x\pm i\sigma_y)/2$, $d(\mathbf{k})$ represents a complex function, and $f(\mathbf{k})$ represents a real function. As an illustration, we consider a generic point $k$ on the $C_6$-invariant axis $[\Gamma-Z(0,0,w)]$ of hexagonal crystal system. Since $[C_{6z},\mathcal{H}(\mathbf{k})]=0$, the band eigenstates at $\mathbf{k}$ can be simultaneously chosen as $C_{6z}$ eigenstates. The little group can be generated by the screw rotation symmetry $\widetilde{C}_{6z}\equiv\{C_{6z}|00\frac{u}{6}\}$, changing the coordinates of the lattice as

$$\widetilde{C}_{6z}:(x,y,z)\to\left(\frac{1}{2}x-\frac{\sqrt{3}}{2}y,\frac{\sqrt{3}}{2}x+\frac{1}{2}y,z+\frac{u}{6}\right), \tag{2}$$

where $u=0,1,2,3,4,5$. Consider a general point located at the $k_z$ axis $(0,0,w)$. Then we can get the relation

$$\widetilde{C}_{6z}^6 = T_{00u} = e^{i2u\pi w}. \tag{3}$$

Hence, the eigenvalues of $\widetilde{C}_{6z}$ can be expressed as

$$E_n=\{e^{in\pi/6}e^{i\pi uw/3}, n=0,2,4,6,8,10\}, \tag{4}$$

where $E_n$ can be used to indicate each phonon branch. When two phonon branches with different eigenvalues cross on this $\widetilde{C}_{6z}$-invariant path, the matrix representation of $\widetilde{C}_{6z}$ can be written as

$$D(\widetilde{C}_{6z})=\begin{pmatrix}E_{n_1} & \\ & E_{n_2}\end{pmatrix}, \tag{5}$$

where $n_1/n_2$ represents different $n$ in Eq. (4). According to the invariant theory, the Hamiltonian of this crossing point can be expressed under the constraint of $\widetilde{C}_{6z}$-invariant symmetry as

$$D(\widetilde{C}_{6z})\mathcal{H}_{eff}(\mathbf{k})D^{-1}(\widetilde{C}_{6z})=\mathcal{H}_{eff}(R_{6z}\mathbf{k}), \tag{6}$$

where $R_{6z}$ is a $3\times3$ rotation matrix of $\widetilde{C}_{6z}$. There exist three possibilities, leading to three types of Weyl points:

$$E_{n_1}/E_{n_2}=e^{\pm i\pi/3},\quad \mathcal{C}=\pm1, \tag{7}$$

$$E_{n_1}/E_{n_2}=e^{\pm 2i\pi/3},\quad \mathcal{C}=\pm2, \tag{8}$$

$$E_{n_1}/E_{n_2}=-1,\quad \mathcal{C}=\pm3. \tag{9}$$

Under the constraint of Eqs. (6) and (9), the crossing point would be a triple Weyl point, and the corresponding Hamiltonian can be expressed as

$$\mathcal{H}_{eff}(\mathbf{k})=\begin{pmatrix}f(\mathbf{k}) & d(\mathbf{k})\\ d^*(\mathbf{k}) & -f(\mathbf{k})\end{pmatrix}, \tag{10}$$

where $f(\mathbf{k})=a_1(k_x^2+k_y^2)+a_2k_z$, $d(\mathbf{k})=\alpha_1k_+^3+\alpha_2k_-^3$, $a_{1,2}$ are real parameters, $\alpha_{1,2}$ are complex parameters, and $k_\pm=k_x\pm ik_y$. In this low-energy effective Hamiltonian, the topological charge of the crossing point is characterized by the leading order of the chiral term (i.e., the antidiagonal term). Besides, the in-plane cubic dispersion originating from the the chiral term is suppressed by the in-plane quadratic dispersion of the nonchiral term (i.e., diagonal term), so the triple Weyl point possesses the in-plane ($k_x$-$k_y$) quadratic dispersion in a spinless system.

Based on the symmetry analysis above, we list the operation eigenvalues of the $C_6$ screw rotation operation at high-symmetry points (HSPs) Γ and A in Table I. Under the action of time-reversal symmetry, two one-dimensional (1D) IRs can form a two-dimensional (2D) IR. For example, when $u=0$ at Γ, $R_{2,6}=R_2\oplus R_6$. In Table I, we list all 2D IRs at high-symmetry Γ and A points, respectively. Then we consider the evolution of two sets of 2D IRs along the HSL Γ-A. The two sets of 2D IRs will split into four 1D IRs along Γ-A. When the screw rotation $6_3$ (i.e., $\widetilde{C}_{6z}$ with $u=3$) is presented, interesting things happen. As shown in Fig. 1(c), two sets of 2D IRs $R_{2,6}$ and $R_{3,5}$ at Γ split into four 1D IRs $R_2$, $R_6$, $R_3$, and $R_5$ along Γ-A, then form two 2D IRs $R_{2,3}$ and $R_{5,6}$ at A. According to the compatibility relations, there must be a crossing with $\mathcal{C}=\pm3$ between $R_3$ and $R_6$. In contrast to the general triple Weyl phonon, this crossing is enforced

TABLE I. IRs of $C_6$ with different screw rotation degrees at high-symmetry points (HSPs) Γ and A, where $u$ represents screw rotation degree. $R_1$, $R_2$, $R_3$, $R_4$, $R_5$, and $R_6$ represent different IRs corresponding to $n = 0$, 2, 4, 6, 8, and 10 in Eq. (4), respectively.

| Degree | HSP | $R_1$ | $R_2$ | $R_3$ | $R_4$ | $R_5$ | $R_6$ | 2D IRs | Triple Weyl on Γ-A |
|---|---|---|---|---|---|---|---|---|---|
| $u=0$ | Γ | 1 | $e^{i\pi/3}$ | $e^{2i\pi/3}$ | $-1$ | $e^{-2i\pi/3}$ | $e^{-i\pi/3}$ | $R_{2,6}$, $R_{3,5}$ | $R_1R_4/R_2R_5/R_3R_6$ |
| | A | 1 | $e^{i\pi/3}$ | $e^{2i\pi/3}$ | $-1$ | $e^{-2i\pi/3}$ | $e^{-i\pi/3}$ | $R_{2,6}$, $R_{3,5}$ | |
| $u=1$ | Γ | 1 | $e^{i\pi/3}$ | $e^{2i\pi/3}$ | $-1$ | $e^{-2i\pi/3}$ | $e^{-i\pi/3}$ | $R_{2,6}$, $R_{3,5}$ | $R_1R_4/R_2R_5/R_3R_6$ |
| | A | $e^{i\pi/6}$ | $i$ | $e^{5i\pi/6}$ | $e^{-5i\pi/6}$ | $-i$ | $e^{-i\pi/6}$ | $R_{1,6}$, $R_{2,5}$, $R_{3,4}$ | |
| $u=2$ | Γ | 1 | $e^{i\pi/3}$ | $e^{2i\pi/3}$ | $-1$ | $e^{-2i\pi/3}$ | $e^{-i\pi/3}$ | $R_{2,6}$, $R_{3,5}$ | $R_1R_4/R_2R_5/R_3R_6$ |
| | A | $e^{i\pi/3}$ | $e^{2i\pi/3}$ | $-1$ | $e^{-2i\pi/3}$ | $e^{-i\pi/3}$ | 1 | $R_{1,5}$, $R_{2,4}$ | |
| $u=3$ | Γ | 1 | $e^{i\pi/3}$ | $e^{2i\pi/3}$ | $-1$ | $e^{-2i\pi/3}$ | $e^{-i\pi/3}$ | $R_{2,6}$, $R_{3,5}$ | $R_1R_4/R_2R_5/R_3R_6$ |
| | A | $i$ | $e^{5i\pi/6}$ | $e^{-5i\pi/6}$ | $-i$ | $e^{-i\pi/6}$ | $e^{i\pi/6}$ | $R_{1,4}$, $R_{2,3}$, $R_{5,6}$ | |
| $u=4$ | Γ | 1 | $e^{i\pi/3}$ | $e^{2i\pi/3}$ | $-1$ | $e^{-2i\pi/3}$ | $e^{-i\pi/3}$ | $R_{2,6}$, $R_{3,5}$ | $R_1R_4/R_2R_5/R_3R_6$ |
| | A | $e^{2i\pi/3}$ | $-1$ | $e^{-2i\pi/3}$ | $e^{-i\pi/3}$ | 1 | $e^{i\pi/3}$ | $R_{1,3}$, $R_{4,6}$ | |
| $u=5$ | Γ | 1 | $e^{i\pi/3}$ | $e^{2i\pi/3}$ | $-1$ | $e^{-2i\pi/3}$ | $e^{-i\pi/3}$ | $R_{2,6}$, $R_{3,5}$ | $R_1R_4/R_2R_5/R_3R_6$ |
| | A | $e^{5i\pi/6}$ | $e^{-5i\pi/6}$ | $-i$ | $e^{-i\pi/6}$ | $e^{i\pi/6}$ | $i$ | $R_{1,2}$, $R_{3,6}$, $R_{4,5}$ | |

by $6_3$ screw rotation symmetry and has an hourglass-type band dispersion structure, which is the THWP. Interestingly, the topological charge of the THWP can be obtained explicitly from the band dispersion without further calculations. In addition, we find that only SGs 173 and 182 satisfy such a symmetry requirement.

Lithium carbonate ($\alpha$-$LiIO_3$) is an ideal candidate to realize the symmetry-enforced THWPs, which is synthesized by reagent grade iodic acid and lithium carbonate dissolved in water [57]. As shown in Fig. 2(a), the SG of $\alpha$-$LiIO_3$ is 173 ($P6_3$), in which a primitive cell contains two Li, two I, and six O atoms. The bulk Brillouin zone (BZ), the projected (001) surface BZ of $\alpha$-$LiIO_3$, and the corresponding HSPs are shown in Fig. 2(b). As shown in Fig. 2(c), we plot the phonon band structure with nonanalytic term correction for $\alpha$-$LiIO_3$. We focus on the nontrivial hourglass crossing on the $C_6$-invariant axis, which corresponds to the THWP. We find that the hourglass crossing contributed from the phonon branches 25 to 28 is an ideal selection. As shown in Fig. 2(d), the THWP has a typical linear dispersion characteristic along the $k_z$ direction. We also plot the corresponding 3D representation of the crossing branches in the $k_x$-$k_y$ plane. It is clear that the crossing point possesses quadratic in-plane dispersion in Fig. 2(e), which is consistent with our model analysis.

We also find six SWPs contributed from 26 and 27 phonon branches at the $k_z = 0$ plane, and the schematic diagram of the momentum positions of two THWPs and six SWPs in the first BZ is shown in Fig. 3(a). Under the rotation of the $C_6$ symmetry operator, these six SWPs are equivalent, and first-principles calculations show that their Chern number is $+1$. According to the no-go theorem, we can also infer that the Chern numbers of the two THWPs along the $k_z$ axis are $-3$. The momentum positions and more detailed information about these nodes are presented in Table S2 of the SM.

Furthermore, in order to explicitly obtain the chirality of THWP, we study the phase difference [i.e., $(3/\pi) \times \arg(E_{n_1}/E_{n_2})$] evolution of the $C_6$ eigenvalues of two phonon branches in Fig. 3(b). We find that there exists a phase change at the $\bar{k}$ point, confirming the existence of a THWP with $\mathcal{C} = -3$. We next examine the distribution of Berry curvature contributed by the 26th and 27th phonon branches in the $k_x$-$k_y$ plane. As shown in Fig. 3(c), the Berry curvature near topological nontrivial points shows convergent and divergent field morphologies, which correspond to the chirality of THWPs and SWPs, respectively.

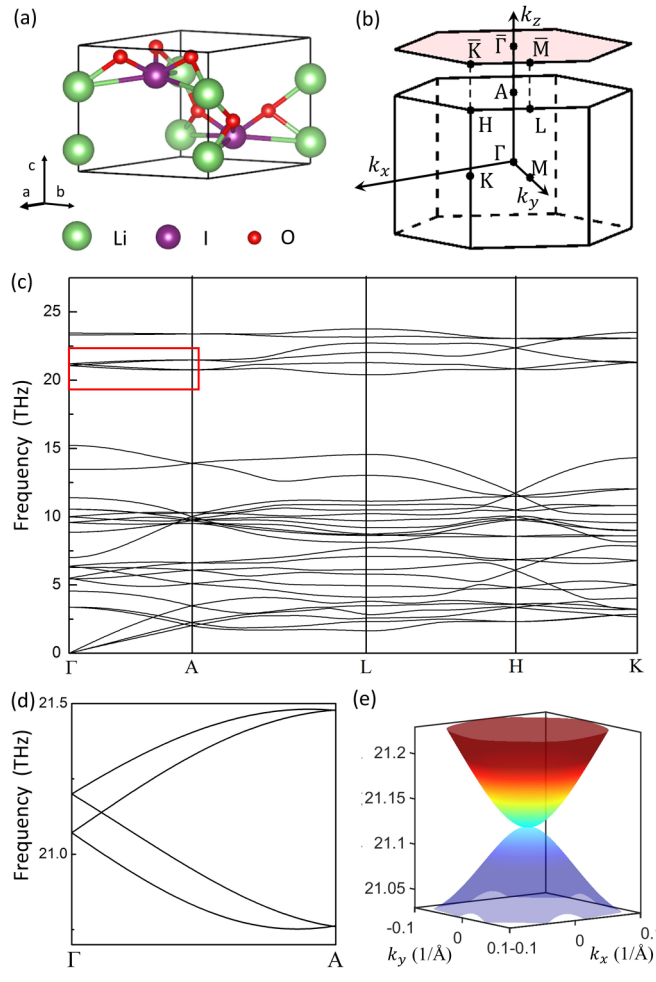


FIG. 2. The crystal structure and phonon band of $LiIO_3$. (a) The primitive cell. (b) The bulk BZ and the corresponding (001) surface BZ. (c) Phonon spectrum. (d) Phonon dispersions along Γ-A contributed from phonon branches 25 to 28, which correspond to the red box in (c). (e) Three-dimensional representation of the phonon dispersion on the $k_x$-$k_y$ plane of the crossing point in (d).

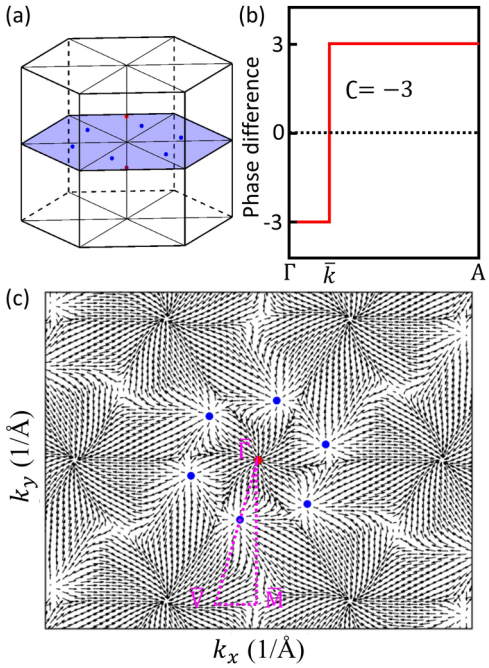


FIG. 3. (a) The distribution of the THWP (red dots) and SWPs (blue dots) in momentum space. (b) The phase difference evolution of $C_6$ rotation operation eigenvalues contributed by two phonon branches 26 and 27 along Γ-A. (c) The distribution of Berry curvature in the $k_x$-$k_y$ plane. $\overline{\Gamma} - \overline{\mathrm{M}} - \overline{\mathrm{V}}$ represents a (001) surface path through the projections of THWPs and SWPs.

To illustrate the exotic topological features of THWPs, we calculate the phonon local density of states (LDOS) and projected isofrequency surface contours on the (001) surface. The phonon surface states, which start at the projection of the THWPs at $\overline{\Gamma}$ and end at the projection of SWPs locating at $\overline{\Gamma}$-$\overline{\mathrm{V}}$, are clearly visible in Fig. 4(a). Moreover, the (001) surface states further display quadratic dispersions of the THWPs, showing consistency with the 3D phonon dispersion in Fig. 2(e). As shown in Fig. 4(b), two THWPs located at Γ-A are projected onto the center of the surface BZ (denoted by $W_1$), forming a terminal point with total $\mathcal{C} = -6$, while the other six SWPs are projected onto the internal general point of the surface BZ (denoted by $W_2$) with $\mathcal{C} = +1$. We can further determine that the six nontrivial terminal points correspond to six SWPs in the isofrequency surface contours with $\omega = 21.37$ THz in Fig. 4(b). And we can see that six branches of surface arcs start at $W_2$, and finally converge at $W_1$. These long surface arcs that connect $W_1$ and $W_2$ exhibit a sextuple-helicoid nature. Unlike the QWPs that usually accompanies the double-helicoid surface state, each THWP induces the simultaneous appearance of three other SWPs, forming the triple-helicoid surface arc structure. The THWPs can only appear on the $C_6$-invariant axis, and its (001) projection is a superposition of two THWPs. Therefore, we can see sextuple-

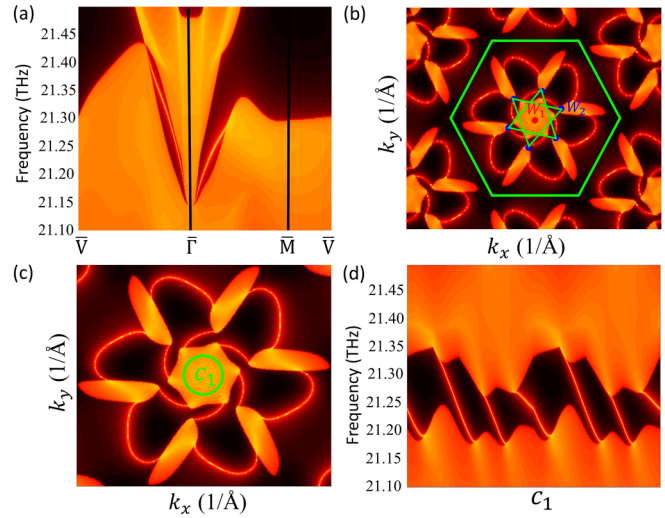


FIG. 4. (a) The phonon LDOS projected on the (001) surface BZ along $\overline{\mathrm{V}}$-$\overline{\Gamma}$-$\overline{\mathrm{M}}$-$\overline{\mathrm{V}}$. (b) The isofrequency contours of (001) surface and (c) its corresponding enlarged view of the middle part at 21.37 THz, where $W_1$ and $W_2$ represent the projection of THWPs and SWPs, respectively. (d) The phonon LDOS projected on the semi-infinite (001) surface BZ along the loop $C_1$.

helicoid surface states, which is in perfect agreement with our theoretical prediction. To visualize the helicoidal surface states, we calculate the surface LDOS along one clockwise loop $C_1$ [see Fig. 4(c)] in Fig. 4(d). For the loop $C_1$, the six left-moving chiral edge modes are consistent with the chirality of $W_1$, further confirming our results.

In summary, we present a class of symmetry-enforced THWP with unique topological properties, which is protected by $6_3$ screw rotation symmetry in chiral SGs 173 and 182. Our work uncovers all THWPs in the spinless system and proposes that their nontrivial surface states connect a THWP with $\mathcal{C} = \pm 3$ and three SWPs with $\mathcal{C} = \mp 1$. In addition, we provide an ideal candidate which possesses two THWPs located at the $C_6$-invariant line and six SWPs located at the $k_z = 0$ plane, leading to sextuple-helicoid surface arcs. The multiple surface arcs can provide one-way phonon propagation channels, suggesting potential applications in topological phonon devices. Our work not only proposes a class of quasiparticles but also provides an idea for detection of unconventional quasiparticles in realistic materials.

*Note added*. Recently, we became aware of a similar work by Wang *et al.* [58].

This work is supported by the National Key R&D Program of China (Grant No. 2022YFA1403700), the National Natural Science Foundation of China (Grant No. 11974160), the Science, Technology, and Innovation Commission of Shenzhen Municipality (Grant No. RCYX20200714114523069), and the Center for Computational Science and Engineering at Southern University of Science and Technology.

[1] A. A. Burkov and L. Balents, Phys. Rev. Lett. **107**, 127205 (2011).

[2] C. Fang, M. J. Gilbert, X. Dai, and B. A. Bernevig, Phys. Rev. Lett. **108**, 266802 (2012).

[3] X. Yuan, Z. Yan, C. Song, M. Zhang, Z. Li, C. Zhang, Y. Liu, W. Wang, M. Zhao, Z. Lin *et al.*, Nat. Commun. **9**, 1854 (2018).

[4] S. Park, Y. Hwang, H. C. Choi, and B. J. Yang, Nat. Commun. **12**, 6781 (2021).

[5] T. Zhang, Z. Song, A. Alexandradinata, H. Weng, C. Fang, L. Lu, and Z. Fang, Phys. Rev. Lett. **120**, 016401 (2018).

[6] H. Miao, T. T. Zhang, L. Wang, D. Meyers, A. H. Said, Y. L. Wang, Y. G. Shi, H. M. Weng, Z. Fang, and M. P. M. Dean, Phys. Rev. Lett. **121**, 035302 (2018).

[7] S. M. Young, S. Zaheer, J. C. Y. Teo, C. L. Kane, E. J. Mele, and A. M. Rappe, Phys. Rev. Lett. **108**, 140405 (2012).

[8] Z. K. Liu, B. Zhou, Y. Zhang, Z. J. Wang, H. M. Weng, D. Prabhakaran, S. K. Mo, Z. X. Shen, Z. Fang, X. Dai *et al.*, Science **343**, 864 (2014).

[9] N. P. Armitage, E. J. Mele, and A. Vishwanath, Rev. Mod. Phys. **90**, 015001 (2018).

[10] X. Cai, L. Ye, C. Qiu, M. Xiao, R. Yu, M. Ke, and Z. Liu, Light: Sci. Appl. **9**, 38 (2020).

[11] Z. J. Chen, R. Wang, B. W. Xia, B. B. Zheng, Y. J. Jin, Y. J. Zhao, and H. Xu, Phys. Rev. Lett. **126**, 185301 (2021).

[12] Y. Kim, B. J. Wieder, C. L. Kane, and A. M. Rappe, Phys. Rev. Lett. **115**, 036806 (2015).

[13] R. Yu, H. Weng, Z. Fang, X. Dai, and X. Hu, Phys. Rev. Lett. **115**, 036807 (2015).

[14] Y. J. Jin, Z. J. Chen, B. W. Xia, Y. J. Zhao, R. Wang, and H. Xu, Phys. Rev. B **98**, 220103(R) (2018).

[15] G. Liu, Y. Jin, Z. Chen, and H. Xu, Phys. Rev. B **104**, 024304 (2021).

[16] Q. F. Liang, J. Zhou, R. Yu, Z. Wang, and H. Weng, Phys. Rev. B **93**, 085427 (2016).

[17] W. Wu, Y. Liu, S. Li, C. Zhong, Z. M. Yu, X. L. Sheng, Y. X. Zhao, and S. A. Yang, Phys. Rev. B **97**, 115125 (2018).

[18] X. Wang, F. Zhou, T. Yang, M. Kuang, Z. M. Yu, and G. Zhang, Phys. Rev. B **104**, L041104 (2021).

[19] X. Wan, A. M. Turner, A. Vishwanath, and S. Y. Savrasov, Phys. Rev. B **83**, 205101 (2011).

[20] A. A. Zyuzin and A. A. Burkov, Phys. Rev. B **86**, 115133 (2012).

[21] D. T. Son and B. Z. Spivak, Phys. Rev. B **88**, 104412 (2013).

[22] X. Huang, L. Zhao, Y. Long, P. Wang, D. Chen, Z. Yang, H. Liang, M. Xue, H. Weng, Z. Fang *et al.*, Phys. Rev. X **5**, 031023 (2015).

[23] H. Weng, C. Fang, Z. Fang, B. A. Bernevig, and X. Dai, Phys. Rev. X **5**, 011029 (2015).

[24] B. Q. Lv, H. M. Weng, B. B. Fu, X. P. Wang, H. Miao, J. Ma, P. Richard, X. C. Huang, L. X. Zhao, G. F. Chen *et al.*, Phys. Rev. X **5**, 031013 (2015).

[25] L. Lu, Z. Wang, D. Ye, L. Ran, L. Fu, J. D. Joannopoulos, and M. Soljačić, Science **349**, 622 (2015).

[26] S. Y. Xu, I. Belopolski, N. Alidoust, M. Neupane, G. Bian, C. Zhang, R. Sankar, G. Chang, Z. Yuan, C. C. Lee *et al.*, Science **349**, 613 (2015).

[27] B. Q. Lv, N. Xu, H. M. Weng, J. Z. Ma, P. Richard, X. C. Huang, L. X. Zhao, G. F. Chen, C. E. Matt, F. Bisti *et al.*, Nat. Phys. **11**, 724 (2015).

[28] B. W. Xia, Y. J. Jin, J. Z. Zhao, Z. J. Chen, B. B. Zheng, Y. J. Zhao, R. Wang, and H. Xu, Phys. Rev. Lett. **122**, 057205 (2019).

[29] A. A. Soluyanov, D. Gresch, Z. Wang, Q. Wu, M. Troyer, X. Dai, and B. A. Bernevig, Nature (London) **527**, 495 (2015).

[30] K. Deng, G. Wan, P. Deng, K. Zhang, S. Ding, E. Wang, M. Yan, H. Huang, H. Zhang, Z. Xu *et al.*, Nat. Phys. **12**, 1105 (2016).

[31] A. Tamai, Q. S. Wu, I. Cucchi, F. Y. Bruno, S. Riccò, T. K. Kim, M. Hoesch, C. Barreteau, E. Giannini, C. Besnard *et al.*, Phys. Rev. X **6**, 031021 (2016).

[32] Z. M. Yu, Y. Yao, and S. A. Yang, Phys. Rev. Lett. **117**, 077202 (2016).

[33] B. W. Xia, R. Wang, Z. J. Chen, Y. J. Zhao, and H. Xu, Phys. Rev. Lett. **123**, 065501 (2019).

[34] Y. J. Jin, Y. Xu, Z. J. Chen, and H. Xu, Phys. Rev. B **105**, 035141 (2022).

[35] B. Zheng, B. Xia, R. Wang, Z. Chen, J. Zhao, Y. Zhao, and H. Xu, Phys. Rev. B **101**, 100303(R) (2020).

[36] X. P. Li, K. Deng, B. Fu, Y. K. Li, D. S. Ma, J. F. Han, J. Zhou, S. Zhou, and Y. Yao, Phys. Rev. B **103**, L081402 (2021).

[37] G. Ding, F. Zhou, Z. Zhang, Z. M. Yu, and X. Wang, Phys. Rev. B **105**, 134303 (2022).

[38] Z. Fang, N. Nagaosa, K. S. Takahashi, A. Asamitsu, R. Mathieu, T. Ogasawara, H. Yamada, M. Kawasaki, Y. Tokura, and K. Terakura, Science **302**, 92 (2003).

[39] S. S. Tsirkin, I. Souza, and D. Vanderbilt, Phys. Rev. B **96**, 045102 (2017).

[40] M. L. Chang, M. Xiao, W. J. Chen, and C. T. Chan, Phys. Rev. B **95**, 125136 (2017).

[41] R. Wang, B. W. Xia, Z. J. Chen, B. B. Zheng, Y. J. Zhao, and H. Xu, Phys. Rev. Lett. **124**, 105303 (2020).

[42] Z. Huang, Z. Chen, B. Zheng, and H. Xu, npj Comput. Mater. **6**, 87 (2020).

[43] Z. M. Yu, Z. Zhang, G. B. Liu, W. Wu, X. P. Li, R. W. Zhang, S. A. Yang, and Y. Yao, Sci. Bull. **67**, 375 (2022).

[44] Y. J. Jin, Z. J. Chen, X. L. Xiao, and H. Xu, Phys. Rev. B **103**, 104101 (2021).

[45] T. Zhang, R. Takahashi, C. Fang, and S. Murakami, Phys. Rev. B **102**, 125148 (2020).

[46] C. Cui, X. P. Li, D. S. Ma, Z. M. Yu, and Y. Yao, Phys. Rev. B **104**, 075115 (2021).

[47] Q. B. Liu, Z. Wang, and H. H. Fu, Phys. Rev. B **103**, L161303 (2021).

[48] H. Li, T. Zhang, A. Said, Y. Fu, G. Fabbris, D. G. Mazzone, J. Zhang, J. Lapano, H. N. Lee, H. C. Lei *et al.*, Phys. Rev. B **103**, 184301 (2021).

[49] H. Nielsen and M. Ninomiya, Nucl. Phys. B **185**, 20 (1981).

[50] H. Nielsen and M. Ninomiya, Nucl. Phys. B **193**, 173 (1981).

[51] L. Wang, S. K. Jian, and H. Yao, Phys. Rev. B **96**, 075110 (2017).

[52] A. Furusaki, Sci. Bull. **62**, 788 (2017).

[53] S. S. Wang, Y. Liu, Z. M. Yu, X. L. Sheng, and S. A. Yang, Nat. Commun. **8**, 1844 (2017).

[54] B. Zheng, F. Zhan, X. Wu, R. Wang, and J. Fan, Phys. Rev. B **104**, L060301 (2021).

[55] Z. J. Chen, Z. J. Xie, Y. J. Jin, G. Liu, and H. Xu, Phys. Rev. Mater. **6**, 034202 (2022).

[56] See Supplemental Material at http://link.aps.org/supplemental/10.1103/PhysRevB.106.214308 for the computational method, momentum positions of triple hourglass Weyl point, and the results of $CaTa_4O_{11}$ (space group 182), which includes Refs. [59–68].

[57] A. Rosenzweig and B. Morosin, Acta Cryst. **20**, 758 (1966).
[58] X. T. Wang, F. Zhou, Z. Y. Zhang, Z. M. Yu and Y. G. Yao, Phys. Rev. B **106**, 214309 (2022).
[59] W. Kohn and L. J. Sham, Phys. Rev. **140**, A1133 (1965).
[60] G. Kresse and J. Furthmüller, Phys. Rev. B **54**, 11169 (1996).
[61] G. Kresse and J. Furthmüller, Comput. Mater. Sci. **6**, 15 (1996).
[62] J. P. Perdew, K. Burke, and M. Ernzerhof, Phys. Rev. Lett. **77**, 3865 (1996).
[63] G. Kresse and D. Joubert, Phys. Rev. B **59**, 1758 (1999).
[64] D. M. Ceperley and B. J. Alder, Phys. Rev. Lett. **45**, 566 (1980).
[65] A. Togo and I. Tanaka, Scr. Mater. **108**, 1 (2015).
[66] Q. Wu, S. Zhang, H. F. Song, M. Troyer, and A. A. Soluyanov, Comput. Phys. Commun. **224**, 405 (2018).
[67] M. P. L. Sancho, J. M. L. Sancho, and J. Rubio, J. Phys. F: Met. Phys. **14**, 1205 (1984).
[68] L. Jahnberg, J. Solid State Chem. **1**, 454 (1970).